ELSEVIER

Journal of Fluids and Structures 24 (2008) 1120–1134

JOURNAL OF FLUIDS AND STRUCTURES

www.elsevier.com/locate/jfs

The transmission of turbulent boundary layer unsteady pressure and shear stress through a viscoelastic layer

D.E. Capone*, W.K. Bonness

Applied Research Laboratory, Pennsylvania State University, P.O. Box 30, State College, PA 16804, USA

Received 7 May 2007; accepted 15 March 2008
Available online 14 July 2008

Abstract

The transmission of unsteady pressure and shear stress, generated by a turbulent boundary layer in water, through a viscoelastic layer backed by a rigid plate is investigated. Analytical models are used to estimate the unsteady pressure and shear stress from 10 to 1000 Hz for a flat plate boundary layer with zero pressure gradient. Additionally, models for the transfer of the unsteady pressures and shear stress through the viscoelastic layer are developed. The models are used to predict the unsteady pressure fluctuations, or flow noise, which would be seen by a finite size sensor embedded under the elastomer layer. The unsteady pressure levels are found to be 20 dB greater than the unsteady shear stress levels across all frequency ranges computed, in agreement with recent measurements. The unsteady pressure transfer functions have a peak at the shear wavenumber and are larger than the shear stress transfer magnitudes from 10 to 50 Hz. The unsteady shear stress transfer functions have a peak at the acoustic wavenumber and are larger than the pressure transfer magnitudes from 50 to 1000 Hz. Over the frequency range examined, the unsteady pressures were found to be the dominant contributor to the sensor flow noise due to the considerably larger magnitude of the unsteady pressures on the top of the viscoelastic layer.

Keywords: Turbulent boundary layer; Unsteady pressure; Unsteady shear; Elastomer

1. Introduction

In many underwater vehicle applications, unsteady pressure transducers are mounted on a steel backing plate and covered with an elastomer layer in order to detect acoustic waves incident on the underwater vehicle (see Fig. 1, for example). Since the purpose of the unsteady pressure transducers is to detect incoming acoustic waves, any other unsteady quantity sensed by the transducer is considered noise. For the application under consideration here, in addition to the incoming acoustic waves, the outer surface of the viscoelastic material is exposed to turbulent flow as the vehicle moves through the water. Therefore, the pressure sensors located underneath the viscoelastic layer are also subjected to unsteady pressure and shear stress fluctuations generated by the turbulent boundary layer (TBL). These fluctuations are considered to be flow noise for acoustic sensing purposes and can also induce vibrations in the steel backing plate resulting in vibration-induced noise on the acoustic sensor. In the interest of understanding and reducing this unwanted noise component, the transmission of TBL unsteady wall pressure and shear stress through an elastomer

*Corresponding author. Tel.: +1 814 863 3027; fax: +1 814 863 5578.
E-mail address: dec5@psu.edu (D.E. Capone).

0889-9746/$ - see front matter © 2008 Elsevier Ltd. All rights reserved.
doi:10.1016/j.jfluidstructs.2008.03.005

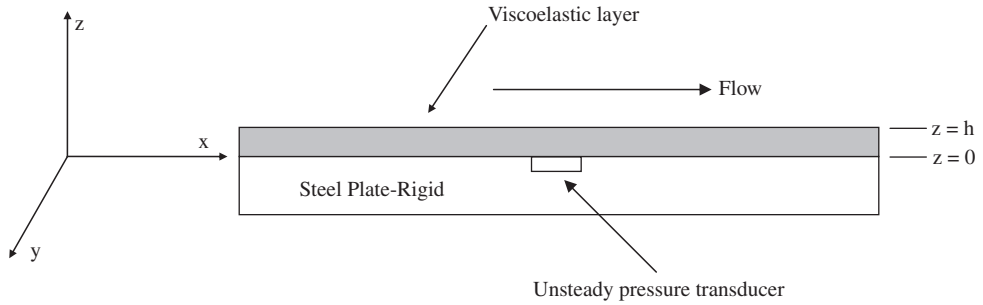

Fig. 1. Coordinate system for viscoelastic and plate system.

layer mounted on a rigid backing plate is studied in this work. Once the unsteady pressure at the surface of the pressure transducer due to the TBL is known, it can be compared to the magnitude of an incoming acoustic wave to determine what, if any, signal-to-noise ratio exists for a given situation.

Frequency ranges, flow velocities, sensor sizes, and elastomer thicknesses of interest in underwater vehicle measurement of acoustic pressures in the presence of TBL-generated flow noise are considered. The normal pressures at a plate/elastomer layer interface generated by a TBL, for a frequency range of 10–1000 Hz and flow speeds of 5, 10 and 15 m/s are computed. In addition, the spatial averaging of unsteady pressures and shear stress due to sensors with radii ranging from 0.05 to 2.54 cm are computed, along with the unsteady pressure and shear stress attenuation due to elastomer layers with thicknesses of 2.54, 5.08 and 7.62 cm.

Previous work in this area, primarily by Ko and Schloemer (1989, 1992), utilized the Corcos (1964) representation of the wavevector frequency spectrum. A more recent model by Chase (1987) is used in this work. The work of Ko and Schloemer did not consider the role of fluctuating shear stress from the TBL, which is the primary emphasis of this current work. In addition, the work of Ko and Schloemer used only the streamwise wavenumber to approximate the value of the in-plane wavenumber in calculating the transmission through a viscoelastic layer. The current work utilizes both streamwise and transverse wavenumbers.

Chase (1993) derived a semi-empirical wavevector–frequency spectrum model of the turbulent wall shear stress. In this model, the low wavenumber content of the fluctuating wall shear stress is comparable in magnitude to the fluctuating wall pressure spectrum. Based upon the model, Chase concludes that the transmission of fluctuating shear stress through a viscoelastic layer may be an important contributor to sensor self-noise for sensors embedded in elastomer layers. In an earlier work, Chase (1991b), discussed the conversion of shear stress to normal stress within an elastomer and derived pressure and shear transfer functions. Again, the conclusion was that the level of the unsteady stress on the surface of the elastomer may contribute to flow noise on a hydrophone.

For this current study, the full two-dimensional Chase (1987) representation of the wavevector–frequency spectrum for unsteady pressure of the TBL is used. A model proposed by Chase (1993) is used to estimate the unsteady shear stress at the surface of the elastomer, so the contribution of the shear stress to the unsteady pressures at the surface of the plate can be computed. Results from the unsteady pressure and shear stress analytical models are compared to experimental data.

Transfer functions used to propagate the unsteady pressure and shear stress through the viscoelastic layer and resolve them as normal forces at the viscoelastic/plate interface are presented. The transfer functions are defined as the ratio of the unsteady pressure at the bottom of the elastomer (surface of the pressure transducer) due to the unsteady pressure or shear stress at the top of the elastomer. Finally, the unsteady pressure models are combined with the transfer functions so that the unsteady pressure (or flow noise) at the sensor surface (located under the elastomer) can be computed for various flow conditions and elastomer layer thicknesses.

2. Unsteady pressure and shear stress models

2.1. Fluctuating wall pressure generated by a turbulent boundary layer

A number of models have been proposed to represent the wavevector–frequency spectrum of turbulent flow over a planar boundary as shown in Fig. 1. These models assume a homogeneous TBL flow at low Mach number over a smooth, stationary plane with zero pressure gradient. In general, researchers used measured autocorrelations and cross-

correlations of the velocity field, along with empirical constants to fit their models to the experimental results. The most commonly utilized models are those by Corcos (1964), Chase (1980), and Chase (1987). More recently, a model by Smolyakov and Tkachenko (1992) has been used by researchers, such as Hambric et al. (2004) and Borisyuk and Grinchenko (1997).

The Corcos model assumes a separable form of the wavevector frequency spectrum, while the Chase (1987) model is non-separable. In general, the Corcos model has been found by researchers to over estimate the low wavenumber (below the convective ridge) region of the spectrum (see for example, Borisyuk and Grinchenko, 1997). Keith and Abraham (1997) examined the reason for the Corcos model over prediction of the low wavenumber region and concluded it was due to the assumption of a constant convection velocity in the model. Capone and Lauchle (1995) found the models by Chase to have good agreement with experimental data for water in a channel flow with a slight modification to one of the model's empirical constants.

Since the purpose of this work is not to compare various models of TBL wall pressure wavevector frequency spectra, the model of Chase (1987) will be used without further discussion. The Chase (1987) model is given by

$$P(k_x,k_y,\omega)=\frac{\rho^2u_*^3}{\left[K_+^2+(b\delta)^{-2}\right]^{5/2}}\left\{\left[c_2\left(\frac{|K_c|}{K}\right)^2+c_3\left(\frac{K}{|K_c|}\right)^2+1-c_2-c_3\right]C_TK^2\left[\frac{K_+^2+(b\delta)^{-2}}{K^2+(b\delta)^{-2}}\right]+C_M\left(\frac{K}{|K_c|}\right)^2k_x^2\right\}, \tag{1}$$

where $P(k_x,k_y,\omega)$ is the two-sided wavenumber, single-sided frequency spectral density of the TBL wall pressure fluctuations, k_x and k_y are the wavenumbers in the x- and y-directions, respectively, $K=\sqrt{k_x^2+k_y^2}$ is the magnitude of the in-plane wavevector, and ρ, u_*, and δ are the fluid density, friction velocity, and boundary layer thickness, respectively. K_c is given by

$$|K_c|^2=\left\{\begin{array}{ll}K^2-\omega^2/c^2, & K>\omega/c\\ \omega^2/c^2-K^2, & K<\omega/c\end{array}\right\}, \tag{2}$$

where c is the speed of sound, and the $(K/|K_c|)$ term in Eq. (1) accounts for compressibility of the fluid, and K_+ is determined from

$$K_+^2=\frac{(\omega-U_ck_x)^2}{(h_{\text{press}}u_*)^2}+K^2, \tag{3}$$

where U_c is the convective velocity. The empirical constants in this model, which Chase suggested by comparison to data from Bull (1967), are

$$h_{\text{press}}=3.0,\quad C_T=0.0047,\quad C_M=0.155,\quad b=0.75,\quad c_2=c_3=0.17. \tag{4}$$

The work of Capone and Lauchle (1995) showed that a value of $b=1.40$ yielded better agreement with data measured in water, and it is used in the following calculations. The one-sided autospectral density of the TBL pressure fluctuations is calculated by the integration of Eq. (1), as performed by Capone and Lauchle (1995),

$$\Phi_{pp}(\omega)=2\int_{-\infty}^{\infty}\int_{-\infty}^{\infty}P(k_x,k_y,\omega)|H(k_x,k_y,\omega)|^2\,\mathrm{d}k_x\,\mathrm{d}k_y, \tag{5}$$

where $H|k_x,k_y,\omega|^2$ is the in-plane wavenumber response function of the measurement sensor. As shown by Ko (1993) for a circular transducer, the in-plane wavenumber response functions is given by

$$|H(k_x,k_y)|^2=\left[\frac{2\mathrm{J}_1((k_x^2+k_y^2)^{1/2}R)}{(k_x^2+k_y^2)^{1/2}R}\right]^2, \tag{6}$$

where J_1 is a Bessel function of the first kind and order one, and R is the radius of the measurement transducer. Similarly, Ko (1993) showed for a rectangular sensor the in-plane wavenumber response is given by

$$|H(k_x,k_y)|^2=\left[\frac{\sin(k_xL_x)}{k_xL_x/2}\cdot\frac{\sin(k_yL_y)}{k_yL_y/2}\right]^2, \tag{7}$$

where L_x and L_y are the dimensions of the sensor in the x- and y-directions, respectively.

2.2. Fluctuating wall shear stress generated by a turbulent boundary layer

The relationship of fluctuating pressure to fluctuating shear stress within the TBL was addressed by Chase (1991a), and a semi-empirical model was proposed by Chase (1993). At low wavenumbers, Chase proposed that the fluctuating wall pressure and shear stress have the same wavevector-white form, and they are totally coherent with a phase difference of $\pi/2$. Chase (1993) also showed that at low wavenumbers the fluctuating shear stress is comparable in magnitude to the fluctuating wall pressure. As discussed previously, given the importance of the low wavenumber region for low Mach number flows in water, the work of Chase (1993) indicates that fluctuating wall shear stress may be an important factor in sensor self-noise for unsteady pressure transducers.

Chase's semi-empirical model for the fluctuating unsteady shear stress is given by

$$S(\omega) = \rho^2 u_*^3 \int_{-\infty}^{\infty}\int_{-\infty}^{\infty} S^+(k_{x+}, k_{y+}, \omega_+)\,\mathrm{d}k_{x+}\,\mathrm{d}k_{y+}, \tag{8}$$

where the subscript plus on a variable indicates it has been non-dimensionalized using inner variables u_* and ν, and S^+ is

$$S^+(k_{x+}, k_{y+}, \omega_+) = B_0\omega_+^{-3/2}(1+m\omega_+)^{-n}\sum_{\pm}(K_{*\pm+}^2/\omega_+)^{-(r+3/2)}, \tag{9}$$

where

$$K_{*\pm+}^2 = \left(\frac{\omega_+ - k_{x+}}{\varepsilon}\right)^2 h^2 + k_{x+}^2 + (k_{z+} \pm \xi_0\omega_+^{1/2})^2 + \alpha_0\omega_+ + (\beta\delta)^{-2}. \tag{10}$$

The empirical constants in Eqs. (9) and (10) are given by

$$B_0 = 0.70\times10^{-4}, \quad m = 3.5, \quad n = 4.0, \quad \varepsilon = 0.11, \quad h_s = 2.0, \quad \xi_0 = 0.1, \quad \text{and} \quad \alpha_0 = 0.0275. \tag{11}$$

Analogous to the wall pressure frequency spectrum, using Eqs. (8)–(11), the spectrum of the wall shear stress fluctuations can be calculated by

$$\Phi_{ss}(\omega) = 2\int_{-\infty}^{\infty}\int_{-\infty}^{\infty} S(k_x, k_y, \omega)|H(k_x, k_y, \omega)|^2\,\mathrm{d}k_x\,\mathrm{d}k_y. \tag{12}$$

Given the frequency spectrum for the unsteady wall pressure, Eq. (5), the magnitude of the normal stress at a given depth in a viscoelastic layer can be calculated as shown by Ko and Schloemer (1992). In the next section, the work of Ko and Schloemer will be expanded such that the transfer function for unsteady shear stress will be derived for the viscoelastic plate system shown in Fig. 1.

2.3. Waves in viscoelastic layers

An incident pressure and/or shear wave on an elastomer layer will result in stresses within the elastomer layer. A transfer function for the propagation of pressure and shear incident on the top of the elastomer layer, $z = h$, through the layer is derived based upon the work by Brekhovskikh (1980) and following the example of Ko and Schloemer (1989, 1992). If one considers waves in the x- and z-directions, the normal and tangential stresses within the elastic layer are:

$$\tau_{zz} = \lambda\left(\frac{\partial u_x}{\partial x} + \frac{\partial u_z}{\partial z}\right) + 2\mu\frac{\partial u_z}{\partial z}, \quad \tau_{zx} = \mu\left(\frac{\partial u_x}{\partial z} + \frac{\partial u_z}{\partial x}\right), \tag{13}$$

where λ and μ are Lamé constants, and u_x and u_z are the normal and tangential displacements, respectively. The displacements are obtained by

$$u_x = \frac{\partial\phi}{\partial x} - \frac{\partial\psi}{\partial z}, \quad u_z = \frac{\partial\phi}{\partial z} + \frac{\partial\psi}{\partial x}, \tag{14}$$

where φ and ψ are the potential functions satisfying the two-dimensional wave equations:

$$\frac{\partial^2\phi}{\partial x^2} + \frac{\partial^2\phi}{\partial z^2} = \frac{1}{c_c^2}\frac{\partial^2\phi}{\partial t^2}, \quad \frac{\partial^2\psi}{\partial x^2} + \frac{\partial^2\psi}{\partial z^2} = \frac{1}{c_s^2}\frac{\partial^2\psi}{\partial t^2}, \tag{15,16}$$

where c_c and c_s are the compressional and shear wave speeds, respectively. The compressional and shear wave speeds are given by

$$c_c = c_{co}(1 - \mathrm{i}\zeta_c)^{1/2}, \quad c_s = c_{so}(1 - \mathrm{i}\zeta_s)^{1/2}, \tag{17}$$

and

$$c_{co} = \left(\mathrm{Re}\left[c_c^2\right]^{1/2}\right), \quad c_{so} = \left(\mathrm{Re}\left[c_s^2\right]^{1/2}\right), \tag{18}$$

where ζ_c and ζ_s are the compressional and shear loss factors, respectively. Assuming a solution of the form (for waves traveling in the positive x-direction)

$$\phi(x,z,t) = \Phi(z)\,\mathrm{e}^{-\mathrm{i}(k_x x - \omega t)}, \quad \psi(x,z,t) = \Psi(z)\,\mathrm{e}^{-\mathrm{i}(k_x x - \omega t)} \tag{19,20}$$

and substituting Eqs. (19) and (20) into Eqs. (15) and (16) yields:

$$\frac{\partial^2 \Phi}{\partial z^2} + (K_{\mathrm{com}}^2 - k_x^2)\Phi = 0, \quad \frac{\partial^2 \Psi}{\partial z^2} + (K_s^2 - k_x^2)\Psi = 0. \tag{21}$$

The quantities $K_{\mathrm{com}} = \omega/c_c$ and $K_s = \omega/c_s$ are the compressional and shear wavenumbers, respectively, in the elastomer layer. Solutions to Eq. (21) are:

$$\Phi = A_1\cos(\alpha z) + A_2\sin(\alpha z), \quad \Psi = A_3\cos(\beta z) + A_4\sin(\beta z), \tag{22}$$

where

$$\alpha = (K_{\mathrm{com}}^2 - k_x^2)^{1/2}, \quad \beta = (K_s^2 - k_x^2)^{1/2}. \tag{23}$$

Assuming the steel backing plate is rigid, the boundary conditions for the solution of Eq. (22) can be determined. At the top surface of the layer, the pressure acting in the normal direction is continuous such that

$$(\tau_{zz})_{z=h} = -(p_0 + \Phi_{pp}), \tag{24}$$

where p_0 is the acoustic pressure satisfying the radiation condition

$$p_0 = A_0\,\mathrm{e}^{(-\alpha_0 z + \mathrm{i}\omega t)} \quad \text{for } z > h, \tag{25}$$

where

$$\alpha_0 = (k_x^2 - k_0^2)^{1/2}, \tag{26}$$

and $k_0 = \omega/c$ is the acoustic wavenumber. The displacement of the elastomer is related to the acoustic pressure by

$$\left.\frac{\partial^2 u_z}{\partial t^2}\right|_{z=h} = -\frac{1}{\rho_0}\left[\frac{\partial p_0}{\partial z}\right]_{z=h}, \tag{27}$$

where u_z is the normal displacement of the elastomer. Using Eqs. (25) and (27) one obtains the result:

$$p_0\big|_{z=h} = -\left[\frac{\rho_0\omega^2}{\alpha_0}\right][u_z]_{z=h}, \tag{28}$$

which results in the first boundary condition

$$\tau_{zz}|_{z=h} = -\Phi_{pp} + \frac{\rho_0\omega^2}{\alpha_0}[u_z]_{z=h}. \tag{29}$$

The shear stress on the surface of the elastomer is given by Eq. (12) and the normal and tangential displacements of at the plate are zero, so the remaining boundary conditions are given by

$$\tau_{zx}(z=h) = \Phi_{ss}, \quad u_z(z=0) = 0, \quad u_x(z=0) = 0. \tag{30}$$

Using Eqs. (13) and (14) and the boundary conditions in Eqs. (29) and (30), a system of linear equations is obtained:

$$\begin{bmatrix} a_{11} & a_{12} & a_{13} & a_{14} \\ a_{21} & a_{22} & a_{23} & a_{24} \\ a_{31} & a_{32} & a_{33} & a_{34} \\ a_{41} & a_{42} & a_{43} & a_{44} \end{bmatrix} \begin{Bmatrix} A_1 \\ A_2 \\ A_3 \\ A_4 \end{Bmatrix} = \begin{Bmatrix} -\alpha_0\Phi_{pp} \\ \Phi_{ss} \\ 0 \\ 0 \end{Bmatrix}, \tag{31}$$

where

$$a_{11} = \rho_e c_s^2 (K^2 - \beta^2)\alpha_0 \cos(\alpha h) + \rho_0 \omega^2 \alpha \sin(\alpha h), \quad a_{12} = \rho_e c_s^2 (K^2 - \beta^2)\alpha_0 \sin(\alpha h) - \rho_0 \omega^2 \alpha \cos(\alpha h),$$
$$a_{13} = 2i\rho_e c_s^2 K\beta\alpha_0 \sin(\beta h) + i\rho_0 \omega^2 k_x \cos(\beta h), \quad a_{14} = -2i\rho_e c_s^2 K\beta\alpha_0 \cos(\beta h) + i\rho_0 \omega^2 k_x \sin(\beta h),$$
$$a_{21} = 2i\rho_e c_s^2 K\alpha \sin(\alpha h), \quad a_{22} = -2i\rho_e c_s^2 K\alpha \cos(\alpha h),$$
$$a_{23} = -\rho_e c_s^2 (K^2 - \beta^2) \cos(\beta h), \quad a_{24} = -\rho_e c_s^2 (K^2 - \beta^2) \sin(\beta h),$$
$$a_{31} = 0, \quad a_{32} = \alpha, \quad a_{33} = -iK, \quad a_{34} = 0, \quad a_{41} = -iK, \quad a_{42} = 0, \quad a_{43} = 0, \quad a_{44} = -\beta, \tag{32}$$

where ρ_e is the density of the elastomer. Finally, the equation for normal stress at the elastomer plate interface due to the unsteady pressure and shear stress on the top of the layer is given by

$$\tau_{zz} = \left[(\rho_e c_s^2 (K^2 - \beta^2) \cos(\alpha z))A_1 + (\rho_e c_s^2 (K^2 - \beta^2) \sin(\alpha z))A_2 \right.$$
$$\left. + (2i\rho_e c_s^2 K\beta \sin(\beta z))A_3 + (-2i\rho_e c_s^2 K\beta \cos(\beta z))A_4\right] \exp(-i(Kx - \omega t)). \tag{33}$$

Eq. (31) is solved to provide the values of $A_1 - A_4$, and the results are used in Eq. (33).

In the next section, Eq. (5) for the pressure spectrum from the TBL, Eq. (12) for the shear stress spectrum from the TBL, and Eq. (33) for the pressure and shear transfer functions are used to calculate the unsteady pressure at the measurement sensor embedded under the elastomer layer using

$$\Phi_{\mathrm{TBL}}(\omega) = 2\int_{-\infty}^{\infty}\int_{-\infty}^{\infty} P(k_x, k_y, \omega)|H(k_x, k_y, \omega)|^2 T(k_x, k_y, \omega)\,\mathrm{d}k_x\,\mathrm{d}k_y + 2\int_{-\infty}^{\infty}\int_{-\infty}^{\infty} S(k_x, k_y, \omega)$$
$$\times |H(k_x, k_y, \omega)|^2 T(k_x, k_y, \omega)\,\mathrm{d}k_x\,\mathrm{d}k_y, \tag{34}$$

where

$$T(k_x, k_y, \omega) = \left|\frac{\tau_{zz}}{\Phi_{pp} \text{ or } \Phi_{ss}}\right|^2. \tag{35}$$

In practice, given the quantity Φ_{TBL}, one can compare its level to that of an incoming acoustic wave to determine if the pressure sensor will detect the acoustic wave over the noise. Typically, the elastomer layers chosen for underwater applications have an acoustic impedance similar to water so that the acoustic pressure transfer function approaches unity.

3. Results

3.1. Comparison to measured data and the effect of transducer size

Measurements of the fluctuating wall pressure from TBLs in water have been made by many researchers, while a much smaller experimental database exists for fluctuating wall shear stress. Some of the most widely referenced shear stress measurements in water have been made by Keith and Bennett (1991) and Colella and Keith (2003). Keith and Bennett (1991) measured unsteady wall pressures in conjunction with unsteady shear stress measurements, providing a good basis for comparison to the semi-empirical models discussed above. Fig. 2 provides a comparison of the Keith and Bennett (1991) data at 6.1 m/s with the predictions of Chase's models. The calculated unsteady pressure levels are corrected for transducer spatial averaging using Eq. (6) and a sensor circular diameter of 0.1 cm, based upon the unsteady pressure sensor used by Keith and Bennett (1991). Likewise, the unsteady shear stress measurements are corrected for transducer spatial averaging using Eq. (7) and streamwise and spanwise lengths of 0.013 and 0.10 cm, respectively. As noted by Keith and Bennett (1991), a nondimensional frequency of 1.4, the unsteady pressure measurements should be attenuated by spatial averaging. Fig. 2 shows that the transducer correction factor from Eqs. (6) and (7) accurately predicted the attenuation caused by the transducers. The agreement between the unsteady pressure model and the data is excellent, while the shear stress model is slightly low at low frequencies. These models provide sufficient accuracy for use in prediction of the effect of the TBL unsteady pressure and stress on a sensor under the elastomer layer.

Using the same flow conditions as the Keith and Bennett experiment, the unsteady pressures which would be measured by sensors of the size often used in underwater applications are calculated. Fig. 3 shows the calculated unsteady pressures for transducers with radii of 0.05, 0.1, 0.64, 1.27 and 2.54 cm. As expected, when the transducer size is larger, the attenuations due to spatial averaging increase with increasing frequency. Clearly, if the intent of a

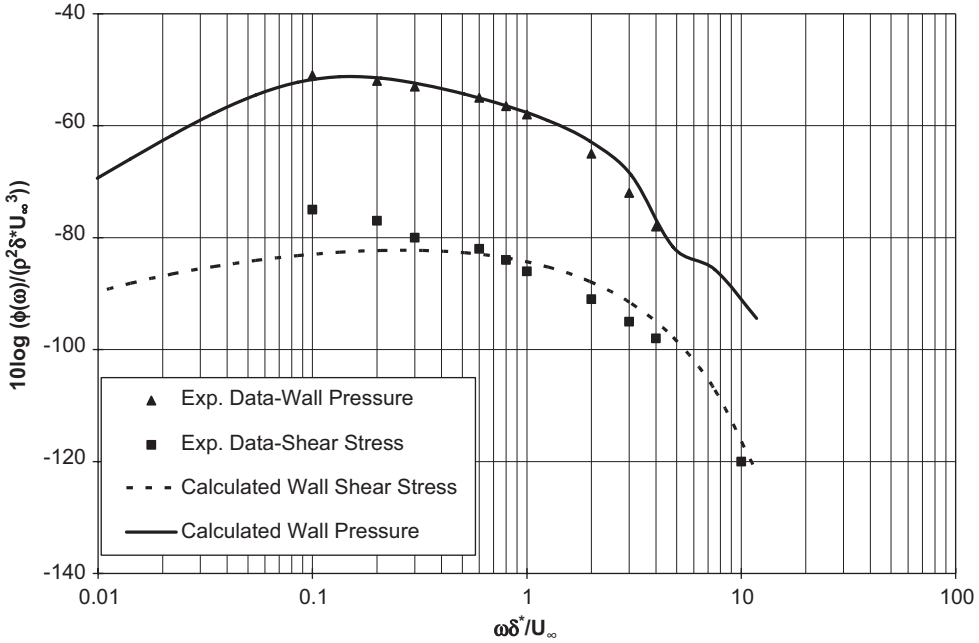

Fig. 2. Comparison of calculated and measured (Keith and Bennett, 1991), unsteady pressure and wall shear stress at 6.1 m/s.

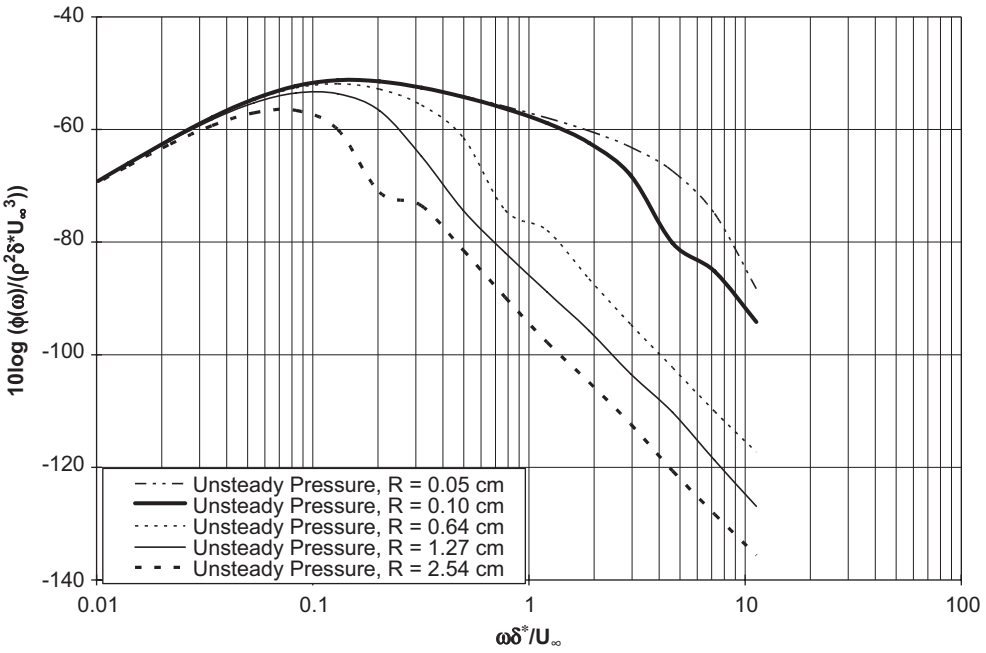

Fig. 3. Comparison of calculated unsteady pressures using the flow conditions of Keith and Bennett with circular transducer of radii 0.05, 0.1, 0.64, 1.27, and 2.54 cm.

measurement is to filter out the high-reduced frequency content of the TBL the use of increasingly larger transducers can be a means to accomplish this goal. The use of larger transducers can be especially helpful for reducing the high-frequency boundary layer noise when one wants to discriminate between it and an incoming acoustic wave.

As the remainder of the results will focus on the effect of the elastomeric layer on the attenuation of the unsteady pressure and shear, the calculations will be performed with a sensor radius of 0.05 cm. A sensor of such a small size will minimize the effect of spatial averaging on the results, so that the following results emphasize the impact of the elastomer layer.

3.2. Unsteady pressure and shear spectra wavenumber transfer functions

Before presenting the integrated results for the normal pressure at the elastomer layer-plate interface, individual component results will be presented for the pressure transfer function, the shear transfer function, the wall pressure spectrum, and the wall shear stress spectrum. Table 1 provides the fluid and viscoelastic properties used in the study.

Fig. 4 shows the change in calculated unsteady pressure and shear on the top surface of the elastomer as a function of flow speed. Both unsteady pressure and shear stress increase as the freestream velocity increases, with the unsteady pressure magnitude at least 20 dB higher than the unsteady shear magnitude.

Fig. 5 shows the unsteady pressure transfer function for a unit pressure, as a function of k_x with $k_y = 0$ for frequencies of 10, 500 and 1000 Hz, and an elastomer thickness of 7.62 cm. Similar to results of Ko and Schloemer (1992), for the 500 and 1000 Hz transfer functions, a peak in the transfer function near the shear wavenumber is

Table 1
Fluid dynamic and material properties used for the study

Parameter	Value(s)
U_∞ (m/s)	5, 10, 15
ρ_0 (kg/m^3)	1000
ρ_e (kg/m^3)	1200
c_{c0} (m/s)	1200
c_{s0}	40
ζ_c	0.3
ζ_s	0.03
Elastomer thickness, h (cm)	7.62, 5.08, 2.54

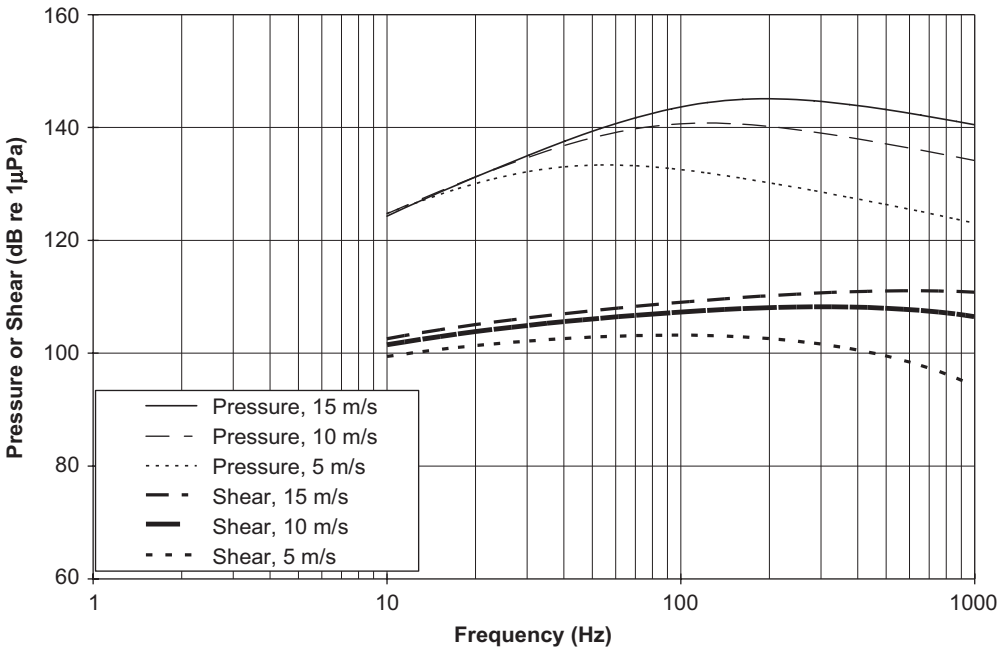

Fig. 4. Unsteady wall pressure and unsteady shear stress for free stream velocities of 15, 10, and 5 m/s.

observed. Fig. 6 shows the shear pressure transfer function for a unit shear force, as a function of k_x with $k_y = 0$ for frequencies of 10, 500 and 1000 Hz, and an elastomer thickness of 7.62 cm. For the shear transfer functions, a peak, similar to that noted by Chase (1993), is observed for 500 and 1000 Hz at the acoustic wavenumber. The acoustic wavenumber for the 10 Hz case is less than the computed wavenumber range of the figure.

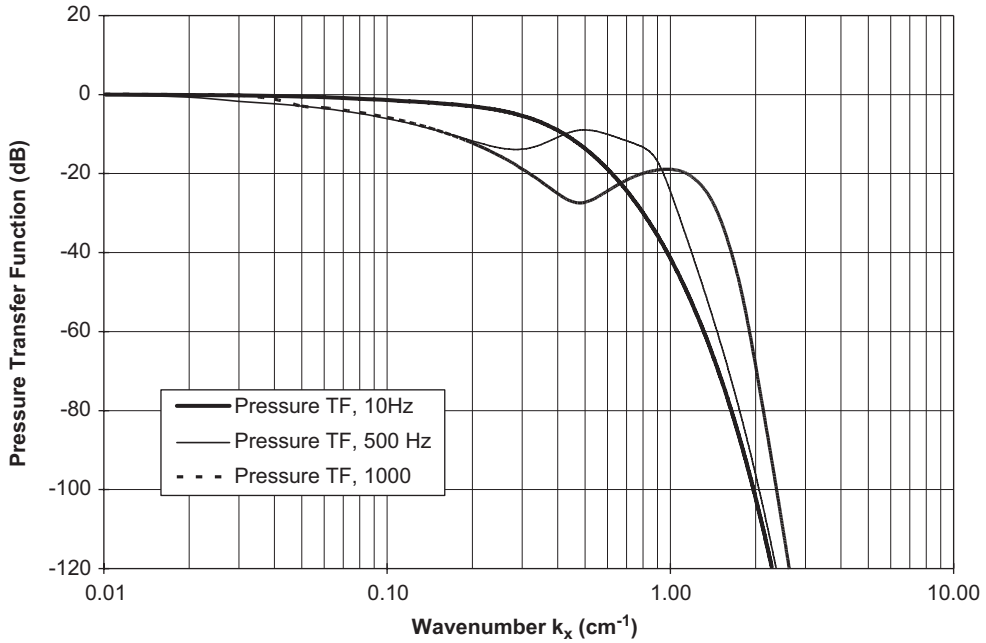

Fig. 5. Pressure transfer functions for a 7.62 cm thick elastomer layer at 10, 500, and 1000 Hz, and flow speed of 15 m/s with $k_y = 0$.

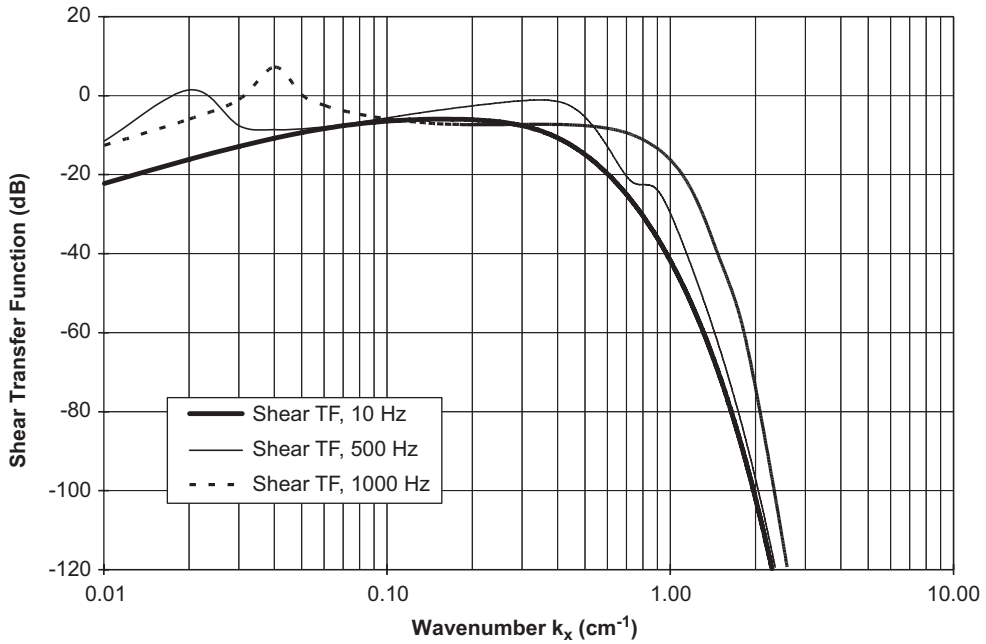

Fig. 6. Shear transfer functions for a 7.62 cm thick elastomer layer at 10, 500, and 1000 Hz, and flow speed of 15 m/s with $k_y = 0$.

Figs. 7 and 8 compare the pressure and shear transfer function for the 7.62 cm thick elastomer at 500 and 1000 Hz, respectively. At the acoustic wavenumber and for wavenumbers between 0.1 and 0.5 cm^{-1} or 1.0 (depending on the frequency), the shear transfer function is of equal or greater magnitude than the pressure transfer function. Chase (1993) noted that, with a rigid backing plate, the conversion from surface shear stress to normal stress at the plate

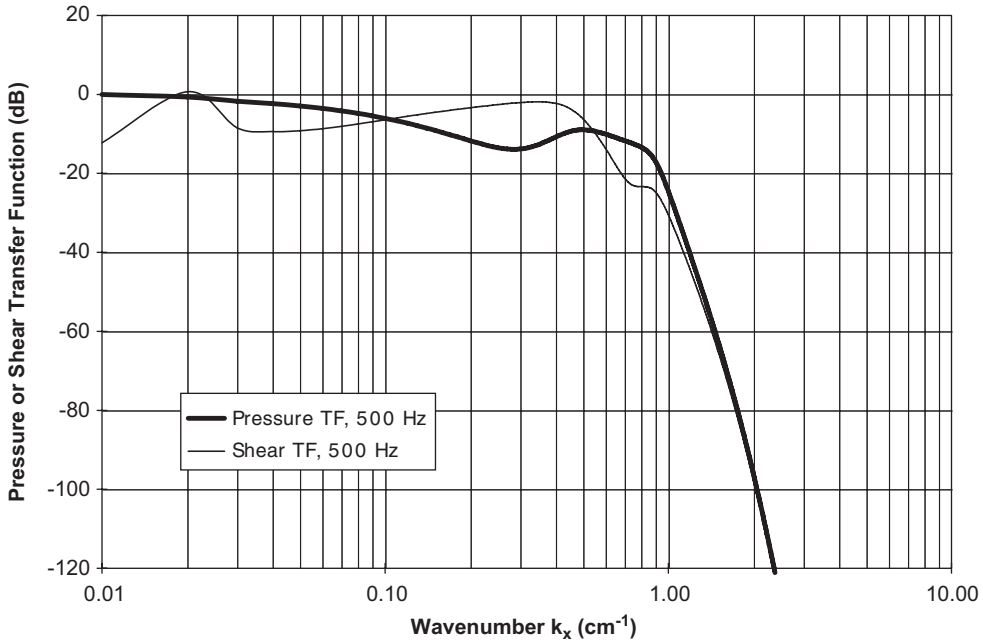

Fig. 7. Pressure and shear transfer functions for a 7.62 cm thick elastomer layer at 500 Hz, and flow speed of 15 m/s with $k_y = 0$.

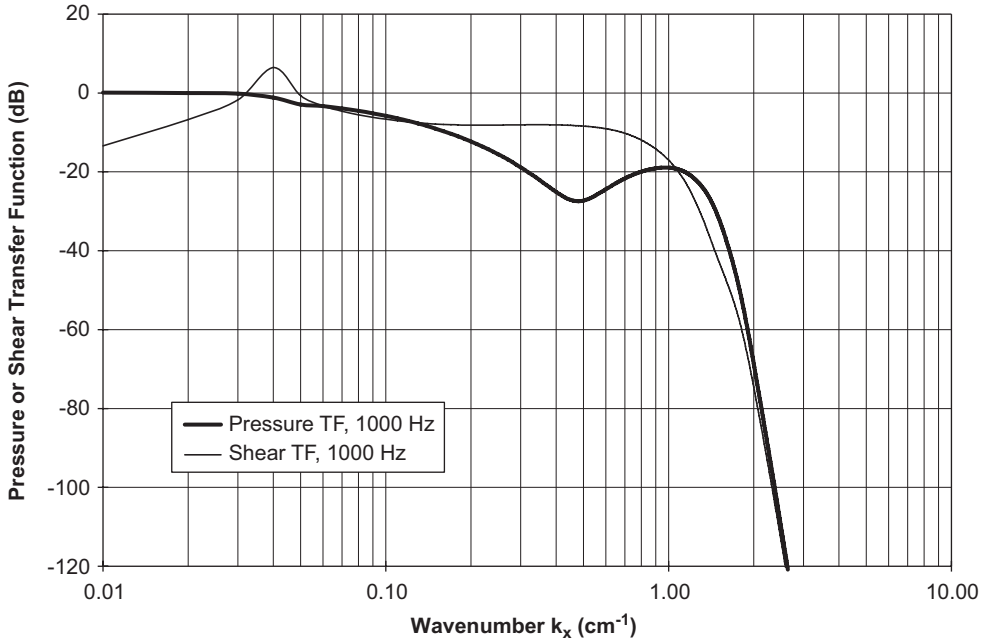

Fig. 8. Pressure and shear transfer functions for a 7.62 cm thick elastomer layer at 1000 Hz, and flow speed of 15 m/s with $k_y = 0$.

surface is enhanced, especially near the acoustic wavenumber. Although not shown, the shear transfer function magnitude at 10 Hz is lower than the pressure transfer function for all wavenumbers.

Fig. 9 shows the shear transfer function for three different elastomer thicknesses, 7.62, 5.08 and 2.54 cm at 15 m/s. As the elastomer layer becomes thinner, more shear is transmitted through the elastomer. Although not shown for brevity,

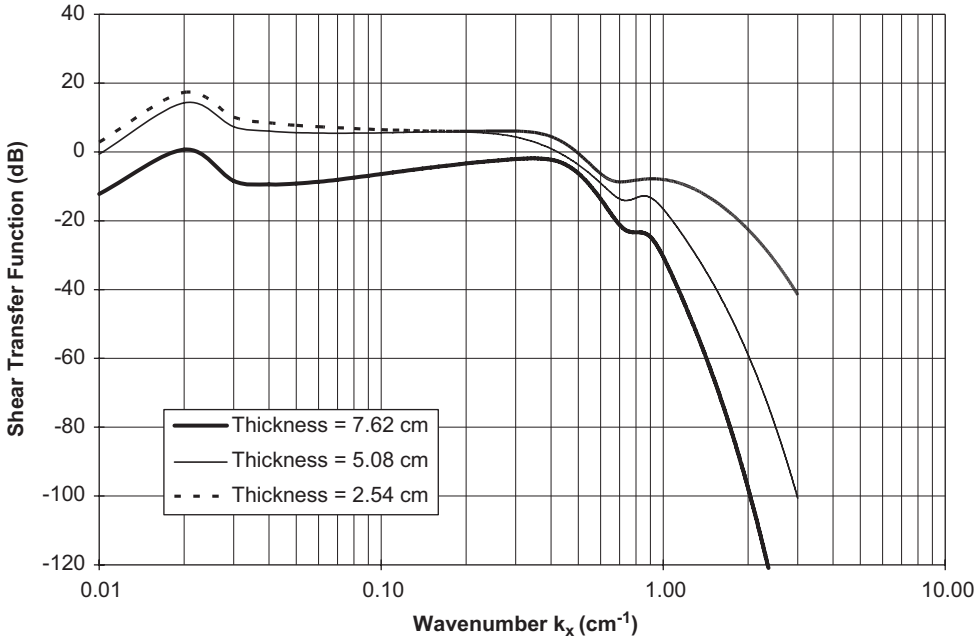

Fig. 9. Shear transfer functions for a 7.62, 5.08, and 2.54 cm thick elastomer layer at 500 Hz, and flow speed of 15 m/s with $k_y = 0$.

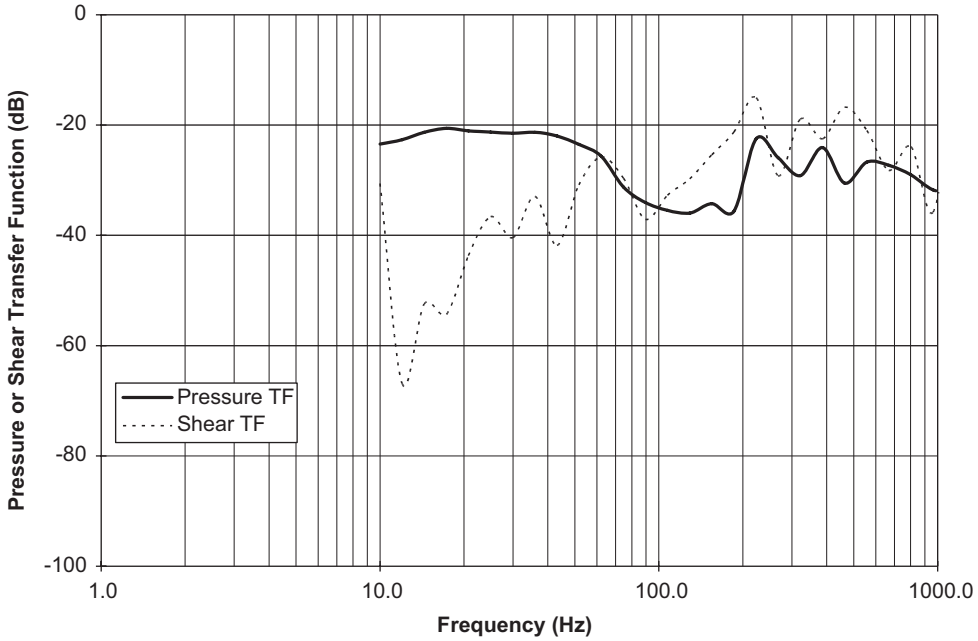

Fig. 10. Frequency-dependent pressure and shear transfer functions for an elastomer thickness of 7.62 cm and flow velocity of 15 m/s.

the pressure transfer functions show the same trend for decreasing elastomer thickness. As one might expect, the results confirm that as the layer becomes thinner, it is less effective in preventing the transmission of the unsteady pressure and shear through the layer.

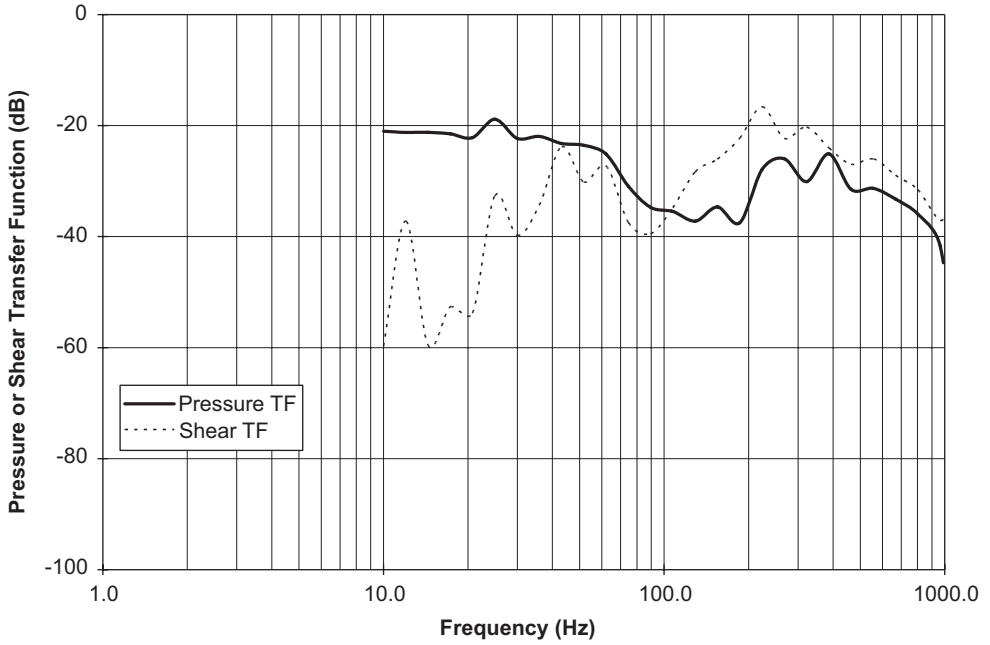

Fig. 11. Frequency-dependent pressure and shear transfer functions for an elastomer thickness of 7.62 cm and flow velocity of 10 m/s.

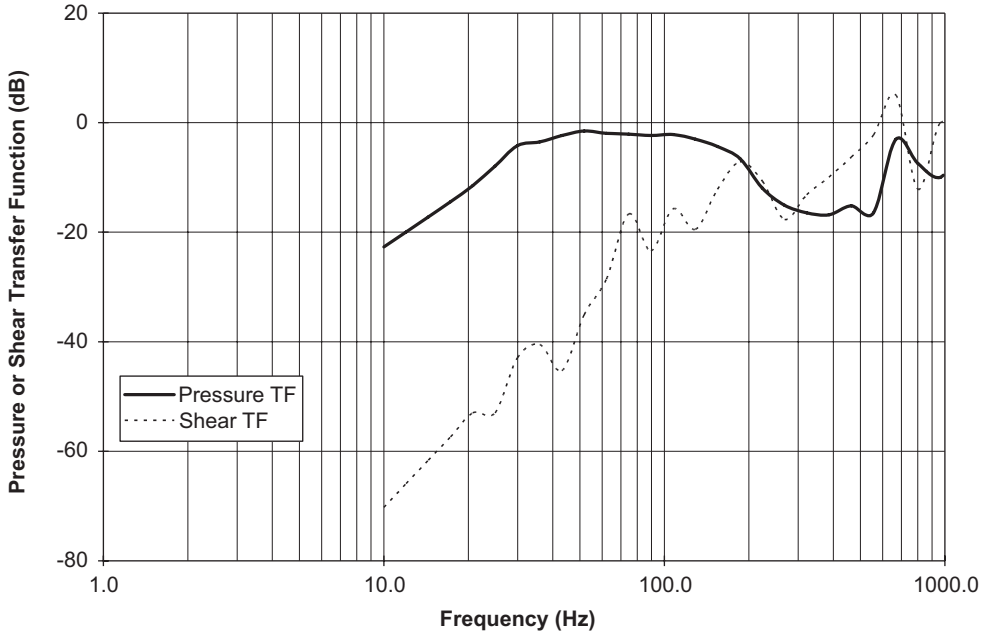

Fig. 12. Frequency-dependent pressure and shear transfer functions for an elastomer thickness of 2.54 cm and flow velocity of 15 m/s.

3.3. Pressure and shear spectra at the surface of the plate

The frequency-dependent pressure and shear transfer functions are shown in Figs. 10 and 11 for an elastomer thickness of 7.62 cm and flow velocities of 15 and10 m/s, respectively. From 10 to 50 Hz, the pressure transfer function is larger than the

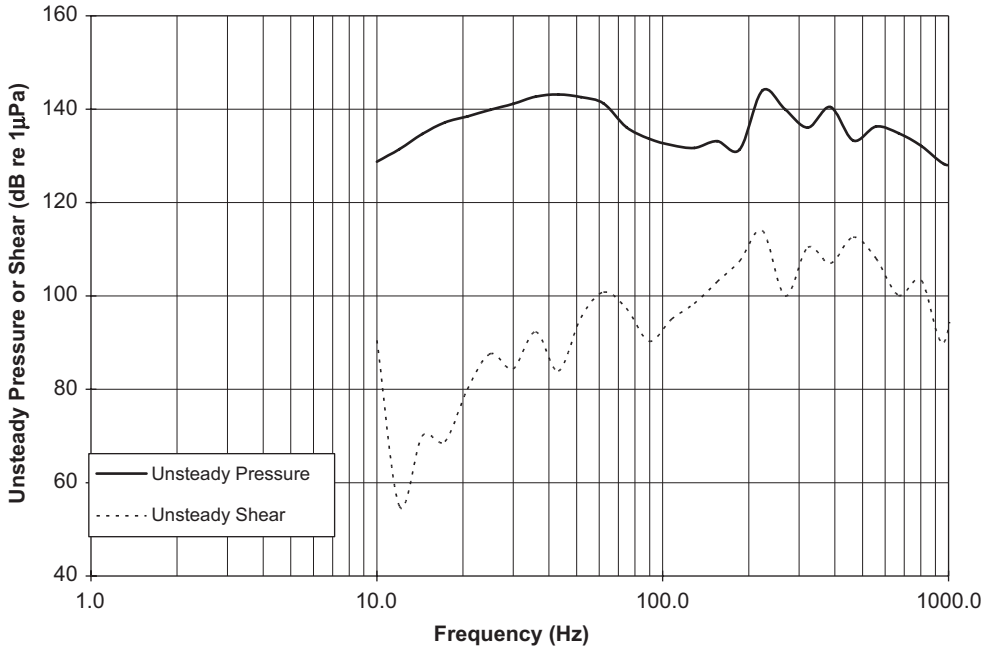

Fig. 13. Unsteady pressure and shear at the rigid plate surface as measured by a sensor with radii of 0.05 cm under a 7.62 cm elastomer layer with a flow velocity of 15 m/s.

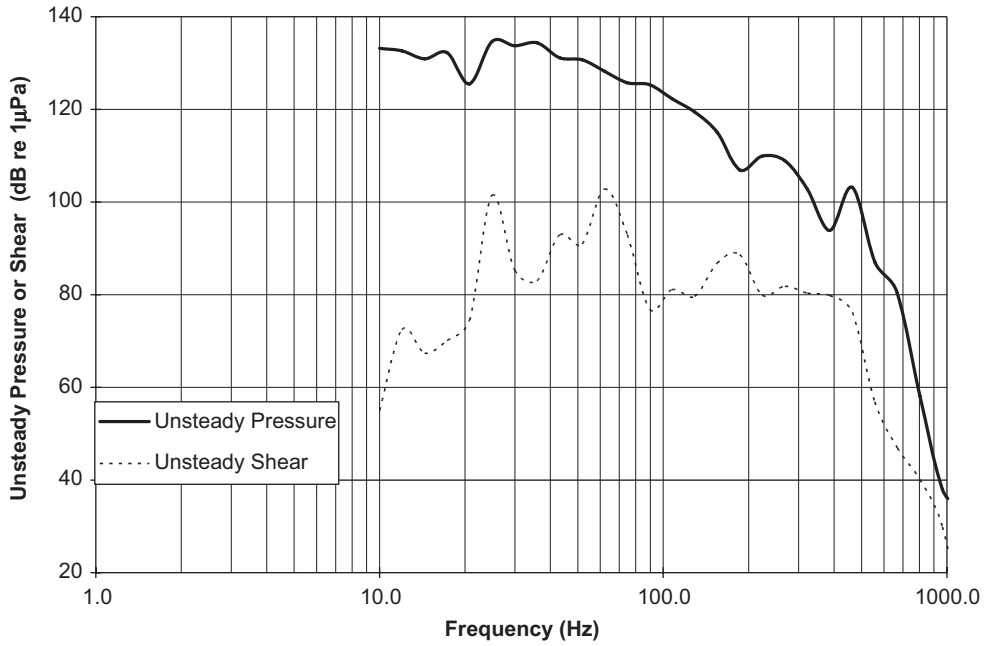

Fig. 14. Unsteady pressure and shear at the rigid plate surface as measured by a sensor with radii of 0.05 cm under a 7.62 cm elastomer layer with a flow velocity of 5 m/s.

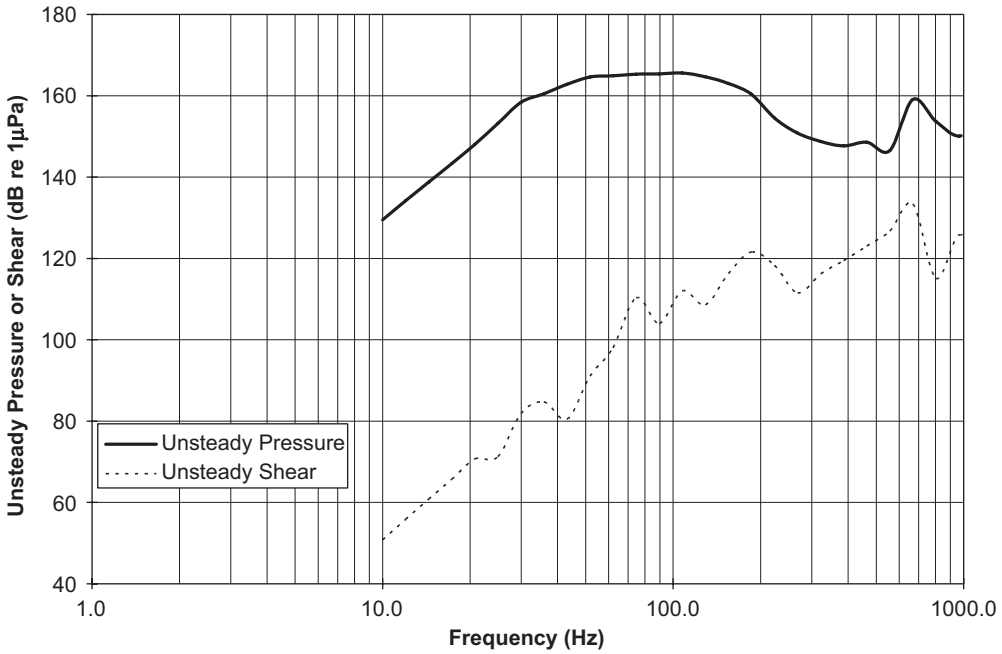

Fig. 15. Unsteady pressure and shear at the rigid plate surface as measured by a sensor with radii of 0.05 cm under a 2.54 cm elastomer layer with a flow velocity of 15 m/s.

shear transfer function, while from 100 to 900 Hz, the shear transfer function magnitude is larger. The transfer function results for 5 m/s are consistent with those for flow speeds of 10 and 15 m/s. Fig. 12 shows the transfer functions for an elastomer layer which is 2.54 cm thick and a flow speed of 15 m/s. For the thinner layer, the pressure transfer function is dominant from 10 to 200 Hz, and the shear transfer function is higher from 300 to 800 Hz. As the elastomer layer becomes thinner, the unsteady pressure and shear transferred from the top to the bottom of the layer is increased. This result is consistent with the results of Ko and Schloemer (1992) for the transmission of unsteady pressure.

Lastly, the unsteady pressure and shear at the bottom of the elastomer layer (the top of the rigid plate) is computed by evaluation of Eq. (34). For all of the results, the measurement sensor is assumed to be a circular transducer with a 0.050 cm active sensing diameter. The unsteady pressure and shear beneath the elastomer measured by a 7.62 cm elastomer layer at 15 m/s is shown in Fig. 13. Across the entire frequency range, 10–1000 Hz, the unsteady pressure generated at the top of the elastomer layer is the dominant noise source as measured by the sensor. By examining Figs. 4 and 10, one can determine why the unsteady pressure controls the noise measured by the sensor. In Fig. 4, it can be seen that the unsteady pressure levels are approximately 30 dB higher than the unsteady shear for the 15 m/s flow velocity. In Fig. 10, it can be seen that the unsteady shear transfer functions are lower than, or at the most, approximately 10 dB higher than the unsteady pressure transfer functions. Fig. 14 shows the same comparison as Fig. 13 for a flow speed of 5 m/s. Similar to the 15 m/s case, the unsteady pressures are the dominant source of noise at the sensor, although at 1000 Hz, the difference in level is approximately 8 dB. The case of a 2.54 cm thick elastomer layer for a flow velocity of 15 m/s is shown in Fig. 15. In this case, an even larger difference exists between the unsteady pressure and shear stress magnitude below 100 Hz. Chase (1991b) also found that at the acoustic wavenumber the conversion from surface shear stress to normal stress is reduced for thinner layers.

4. Summary and conclusions

In this work, the unsteady pressure and shear stress on the top of an elastomer layer from a TBL in water are calculated using two-dimensional wavevector–frequency models. The calculated values are used in conjunction with derived pressure and shear transfer functions to estimate the flow noise on a sensor embedded under the elastomer layer backed by a rigid plate. Results are computed for a variety of flow speeds, elastomer thicknesses, and sensor sizes.

A comparison between the two-dimensional TBL model of the unsteady shear stress proposed by Chase (1993) and the measurements of Keith and Bennett (1991) shows a favorable comparison. As previously verified, the unsteady

pressures predicted by the model agree with measurements of the unsteady pressure. The unsteady pressures predicted are found to be between 20 and 35 dB higher than the unsteady shear stress for the flow conditions considered between 10 and 1000 Hz. It is also shown that, as the sensor size increases, the measured high-reduced frequency content of the TBL decreases due to increased sensor spatial averaging.

Transfer functions for the transmission of unsteady pressure and unsteady shear to normal pressure through an elastomer layer are derived. The unsteady pressure and shear transfer functions are computed as a function of wavenumber, k_x. The unsteady shear transfer functions have a peak at the acoustic wavenumber, while the unsteady pressure transfer functions have a peak near the shear wavenumber. The transfer functions are integrated over both k_x and k_y to provide results as a function of frequency. In general, the transfer functions for pressure are 20–40 dB higher at frequencies less than 100 Hz. Above 100 Hz, the unsteady shear transfer functions are 0–10 dB higher. As the thickness of the covering elastomer layer increases, the pressure or shear transmitted through the layer decreases.

Contributions to the sensor flow noise are computed for a TBL due to unsteady shear stress and unsteady pressure. For the frequency range of 10–1000 Hz, and for all of the flow velocities and elastomer thicknesses examined, the unsteady pressures are the dominant contributor to the sensor flow noise. This unsteady pressure is the dominant contributor due to the relatively high level of unsteady pressure and relatively low unsteady shear stress on the surface of the elastomer layer and the similarity in levels of the pressure and shear stress transfer functions above 100 Hz.

References

Borisyuk, A.O., Grinchenko, V.T., 1997. Vibration and noise generation by elastic elements excited by a turbulent flow. Journal of Sound and Vibration 204 (2), 213–237.

Brekhovskikh, L.M., 1980. Waves in Layered Media, second ed. Academic Press, San Diego, CA.

Bull, M.K., 1967. Wall-pressure fluctuations associated with subsonic turbulent boundary layer flow. Journal of Fluid Mechanics 28, 719–754.

Capone, D.E., Lauchle, G.C., 1995. Calculation of turbulent boundary layer wall pressure spectrum. Journal of the Acoustical Society of America 98 (4), 2226–2234.

Chase, D.M., 1980. Modeling the wavevector-frequency spectrum of turbulent boundary layer wall pressure. Journal of Sound and Vibration 70 (1), 29–67.

Chase, D.M., 1987. The character of the turbulent wall pressure spectrum at subconvective wavenumbers and a suggested comprehensive model. Journal of Sound and Vibration 112 (1), 125–147.

Chase, D.M., 1991a. Fluctuations in wall-shear stress and pressure at low streamwise wavenumbers in turbulent boundary-layer flow. Journal of Fluid Mechanics 225, 545–555.

Chase, D.M., 1991b. Generation of fluctuating normal stress in a viscoelastic layer by surface shear-stress and pressure as in turbulent boundary-layer flow. Journal of the Acoustical Society of America 89 (6), 2589–2596.

Chase, D.M., 1993. A semi-empirical model for the wavevector-frequency spectrum of the turbulent wall-shear stress. Journal of Fluids and Structures 7, 639–659.

Colella, K.J., Keith, W.L., 2003. Measurements and scaling of wall shear stress fluctuations. Experiments in Fluids 34, 253–260.

Corcos, G.M., 1964. The structure of the turbulent pressure field in boundary layer flows. Journal of Fluid Mechanics 18, 353–378.

Hambric, S.A., Hwang, Y.F., Bonness, W.K., 2004. Vibrations of plates with clamped and free edges excited by low-speed turbulent boundary layer flow. Journal of Fluids and Structures 19, 93–110.

Keith, W.L., Abraham, B.M., 1997. Effects of convection velocity and decay of turbulence on the wall pressure wavenumber-frequency spectrum. ASME Journal of Fluids Engineering 119, 50–55.

Keith, W.L., Bennett, J.C., 1991. Low-frequency spectra of the wall shear stress and wall pressure in a turbulent boundary layer. AIAA Journal 29, 526–530.

Ko, S.H., 1993. Performance of various shapes of hydrophones in the reduction of turbulent flow noise. Journal of the Acoustical Society of America 93, 1293–1299.

Ko, S.H., Schloemer, H.H., 1989. Calculations of turbulent boundary layer pressure fluctuations transmitted into a viscoelastic layer. Journal of the Acoustical Society of America 85 (4), 1469–1477.

Ko, S.H., Schloemer, H.H., 1992. Flow noise reduction techniques for a planar array of hydrophones. Journal of the Acoustical Society of America 92 (6), 3409–3424.

Smolyakov, A.V., Tkachenko, V.M., 1992. Model of a field of pseudosonic turbulent wall pressure and experimental data. Soviet Physics-Acoustics 37, 627–631.